[논 문] 한국재료학회지
Korean J. Mater. Res.
Vol. 31, No. 8 (2021)

https://doi.org/10.3740/MRSK.2021.31.8.445

Improvement of Thermoelectric Properties in Te-Doped Zintl Phase Magnesium-Antimonide

Md. Mahmudur Rahman and Soon-Chul Ur†

Dept. of Material Sci. and Eng., Research Center for Sustainable Eco-Devices and Materials (ReSEM), Korea National University of Transportation, Chungju, Chungbuk 27469, Republic of Korea

(Received July 14, 2021 : Revised August 9, 2021 : Accepted August 10, 2021)

Abstract Zintl compound Mg_3Sb_2 is a promising candidate for efficient thermoelectric material due to its small band gap energy and characteristic electron-crystal phonon-glass behavior. Furthermore, this compound enables fine tuning of carrier concentration via chemical doping for optimizing thermoelectric performance. In this study, nominal compositions of $Mg_{3.8}Sb_{2-x}Te_x$ ($0 \leq x \leq 0.03$) are synthesized through controlled melting and subsequent vacuum hot pressing method. X-ray diffraction (XRD) and scanning electron microscopy (SEM) are carried out to investigate phase development and surface morphology during the process. It should be noted that 16 at. % of excessive Mg must be added to the system to compensate for the loss of Mg during melting process. Herein, thermoelectric properties such as Seebeck coefficient, electrical conductivity, and thermal conductivity are evaluated from low to high temperature regimes. The results show that Te substitution at Sb sites effectively tunes the majority carriers from holes to electrons, resulting in a transition from p to n-type. At 873 K, a peak ZT value of 0.27 is found for the specimen $Mg_{3.8}Sb_{1.99}Te_{0.01}$, indicating an improved ZT value over the intrinsic value.

Key words zintl phase, Mg_3Sb_2, Te doped, controlled melting.

1. Introduction

Thermoelectric devices can convert electricity into thermal energy and vice versa as the temperature changes.[1] The dimensionless figure of merit ZT determines the efficiency of thermoelectric materials. The following equation can be used to calculate the ZT value.

$$ZT = \frac{S^2\sigma}{\kappa}T \quad (1)$$

In this equation, S denotes the Seebeck coefficient, σ is the electrical conductivity, κ is the thermal conductivity, and T denotes the temperature in Kelvin. As demonstrated in eq. (1), a high ZT value requires a high power factor (PF), $S^2\sigma$, and low thermal conductivity (κ). According to the Widemann-Franz law, electrical conductivity is directly proportional to electronic thermal conductivity ($\kappa_E = \sigma LT$, where κ_E is electronic thermal conductivity and L is Lorenz number).[2] Furthermore, as carrier concentration rises, the Seebeck coefficient falls while electrical conductivity rises. These interdependencies make achieving high ZT challenging. As a result, an optimal value of S, σ and κ are required to obtain a high dimensionless figure of merit (ZT). In order to obtain a high ZT value, various strategies were used, which either reduced thermal conductivity by increasing phonon scattering[3,4] or increased electronic properties by tuning the carrier concentration.[5,6]

In many ways, Zintl phases exhibit desirable TE properties due to their small-band-gap, as well as diverse and complex crystal structures[7]. Their rich crystal chemistry allows for precise tuning of transport properties. The semiconducting nature of Zintl phases is due to their valence compound behavior. Such phases contain elements with high electronegativity differences, resulting in a clear distinction between anionic and cationic parts, with electron transfer from one to the other assumed to be essentially complete.[7] Generally, Zintl compounds have two ionic sites, one of which is an electropositive cation, and the other an electronegative anion.[8] The electropositive cation can donate electrons to the electronegative anion, resulting in an ionic compound. Furthermore, if

†Corresponding author
E-Mail : scur@ut.ac.kr (S.-C. Ur, Korea Nat'l Univ. of Transportation)

the cation accommodates an insufficient number of electrons to donate anion, the anion's valance shell will be incomplete. As a result, anion forms a covalent bond with another anion. The presence of both ionic and covalent bonds complicates the structure of zintl compounds, resulting in electron-crystal phonon-glass properties.[9)]

The zintl compound Mg_3Sb_2 has two structures: cubic and hexagonal.[7)] The cubic α-Mg_3Sb_2 is a low temperature phase composed of 48 Mg and 32 Sb atoms, similar to the structure of α-La_2O_3. However, the hexagonal crystal structure of Mg_3Sb_2 is known as β-Mg_3Sb_2, a high temperature phase similar to the crystal structure of Mn_2O_3. It has two distinct Mg sites where ionic Mg^{2+} cation can donate electron to $[Mg_2Sb_2]^{2-}$ sites, resulting in typical zintl compound behavior.[9)]

P-type Mg_3Sb_2 demonstrated poor thermoelectric performance due to their low electrical properties, which limited its practical application. Numerous experiments have conducted to improve the ZT value of p-type Mg_3Sb_2, but it remains less than one.[10-14)] However, due to their low thermal conductivity and high electrical properties, n-type Mg_3Sb_2 demonstrated high thermoelectric performance.[7,9,15,16)] In this study, a small amount of Te was introduced at Sb sites to investigate the effect of Te doping in the solid solution of $Mg_{3.8}Sb_{2-x}Te_x$ on the subsequent thermoelectric properties. A theoretical calculation has shown that Te can act as an effective n-type dopant because the formation energy of Te interstitials is relatively lower when compared to Mg interstitials.[17)]

In this study, Mg_3Sb_2 alloying with variable Te composition ($0 \le x \le 0.03$) were synthesized using a controlled melting method that included elemental shots, pulverizing, and vacuum hot pressing (VHP). This procedure is very novel for this type of alloy system and reduced the overall processing times.[18,19)] In order to produce single-phase Mg_3Sb_2, an excessive amount of Mg was considered to be added in the initial powder mixture, because the composition of the nominally designed Mg_3Sb_2 usually resulted in excessive Sb contents after the hot consolidation process, as reported in other studies.[20)] It was reported that Te doped Mg_3Sb_2, synthesized via levitation melting, ball milling followed by spark plasma sintering, turned out to be n-type conduction and showed improved thermoelectric properties in the Mg_3Sb_2.[11)] This study also showed that Te doping in $Mg_{3.8}Sb_{2-x}Te_x$ ($0 \le x \le 0.03$) improved electrical conductivity as well as Seebeck coefficient while decreasing thermal conductivity, resulting in a higher ZT value than that of pristine state.

2. Materials and Method

All samples with the nominal composition $Mg_{3.8}Sb_{2-x}Te_x$ ($0 \le x \le 0.03$) were prepared and mixed using elemental shots of Mg (99.9 % purity, Kojundo), Sb (99.999 % purity, Kojundo), and Te (99.9 % purity, Kojundo). For controlled melting, the measured sample was placed in a graphite crucible with a stopper, the inner walls of which were coated with a thick layer of boron nitride (BN). The crucible was then placed in the vacuum furnace. The sample was then heated for 1 h at 1,173 °C. After the heating process was completed, the cooled ingot was pulverized with a mortar pestle. The powders were also sieved using a 325 mesh sieve. The entire pulverizing to sieving process was carried out under Ar gas atmosphere in a glove box. Then, vacuum hot pressing (VHP) was carried out at 70 MPa and 873 K for 4 h. The phases were characterized by X-ray diffraction (XRD; Bruker AXS Advance D-8, Germany) of a Cu-Kα radiation. Scanning electron microscopy (SEM, FEI Quanta-400, Netherland) was carried out to study particle size, and surface morphology. The electronics property in terms of electrical conductivity and Seebeck coefficient were estimated using the 4-probe method inserted into ZEM-III (Ulvac-Riko, Japan). The VHPed samples were cut into cylindrical samples of $3 \times 3 \times 9$ mm^3 for this calculation. Circle samples of $10\Phi \times 1$ mm were produced to measure thermal diffusivity using laser flash process within TC-9000H (Ulvac-Riko, Japan). The density for all prepared sample was determined by Archimedes principle where distilled water was used. The Van der Pauw technique (modified Keithley 7065, USA) was conducted to measure the transport properties at a fixed magnetic field (1T) and fixed electric current (10 mA).

3. Result and Discussion

X-ray diffraction (XRD) data for VHPed $Mg_{3.8}Te_xSb_{2-x}$ is shown in Fig. 1(a). As a reference, XRD data for x = 0.02 after casting is plotted in this figure. From the figure it can be observed that no secondary phases are appeared. Fig. 1(b) depicts lattice parameters a, and c for VHPed $Mg_{3.8-x}Te_xSb_{2-x}$ as a function of Te concentration (x). With increasing x, lattice parameters are observed to decrease. Due to lower ionic radii of Te^{2-} than that of Sb^{3-}, substitution of Te at Sb sites may increase the lattice parameter.[21)] This could imply that Te was induced by the lattice position of Sb.

Fig. 2(a) shows the microstructure of pulverized powders for $Mg_{3.8}Te_{0.01}Sb_{1.99}$. The particles were typically angular in shape and less than 45 μm in diameter since samples were sieved through 325 meshes after pulverization. The surface morphology of the fractured sample for VHPed $Mg_{3.8}Te_{0.01}Sb_{1.99}$ is shown in Fig. 2(b). As can be seen, the sample has a dense microstructure with no obvious internal flaws. The characteristics of the lamellar structure are commonly observed in this material system, as well

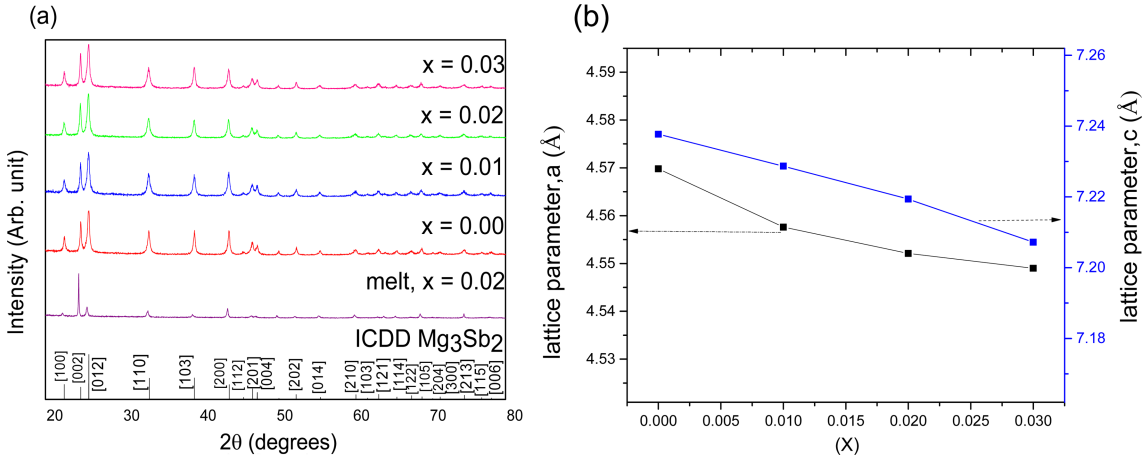

Fig. 1. XRD diffraction pattern of $Mg_{3.8}Te_xSb_{2-x}$ for (a) VHPed sample and (b) lattice parameter with respect to Te content (x).

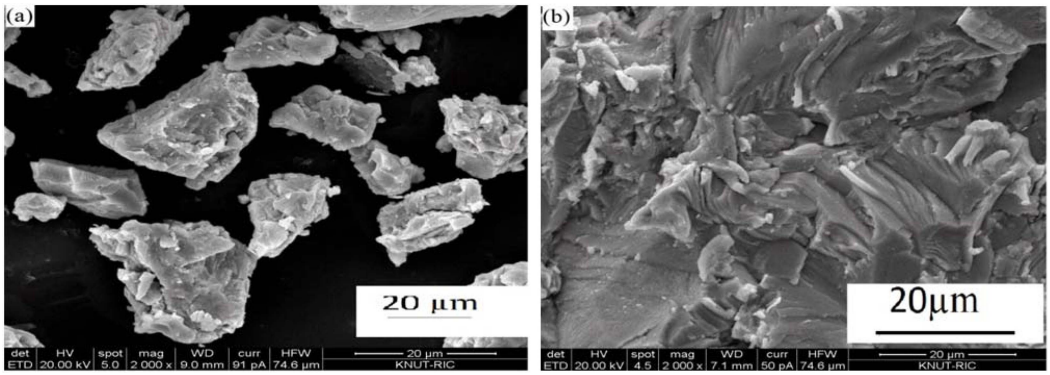

Fig. 2. Scanning electron microscopy of (a) as-sieved and (b) fractured surface of VHPed $Mg_{3.8}Te_{0.01}Sb_{1.99}$.

as in other studies.[22] Energy dispersive X-ray spectroscopy (EDS) line profile for VHPed $Mg_{3.8}Te_{0.01}Sb_{1.99}$ is shown in Fig. 3. Te seems to be uniformly distributed within the detected area.

The electrical conductivity of the samples $Mg_{3.8}Te_xSb_{2-x}$ ($0 \leq x \leq 0.03$) is shown in Fig. 4(a). As it can be seen, the electrical conductivity is increased with increasing temperature, corresponding to intrinsic semiconductor behavior. At room temperature, all compositions have a high electrical resistivity. These semiconductors, however, exhibit an increase in electrical conductivity beyond 373 K. It is believed that the majority carrier (electrons) gains enough energy to cross the band gap region at 373 K. It can also be observed that maximum σ for Te doped samples is lower than the intrinsic one, possibly due to decrease in carrier mobility.

Fig. 4(b) depicts the variation of the Seebeck coefficient for the synthesized pellets. The Seebeck coefficient found to be negative in all of the Te-doped samples, indicating the n-type semiconductor properties with respect to Hall coefficient measurement, as shown in Table 1. This employs that the primary carrier type is turned into free

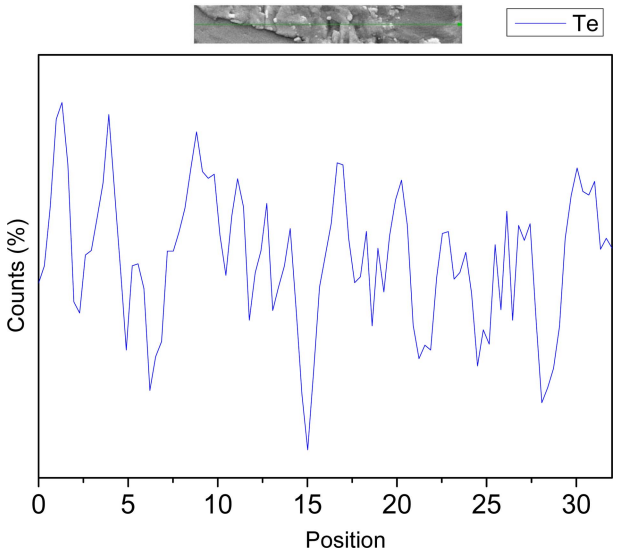

Fig. 3. EDS line profile showing homogeneous Te distribution in the matrix for x = 0.01.

electrons when Te doping takes place. In terms of temperature, and magnitude, the Seebeck coefficients of

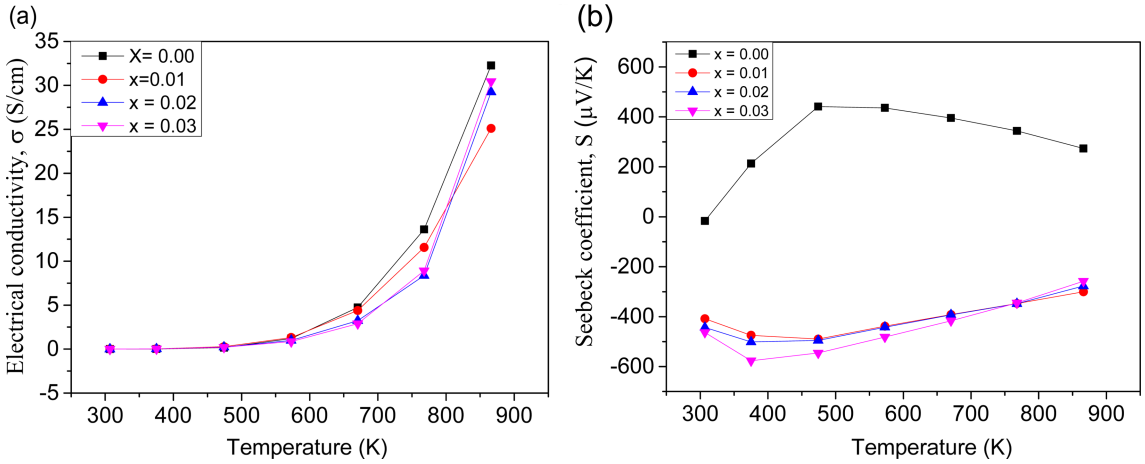

Fig. 4. Temperature dependence (a) electrical conductivity, (b) Seebeck coefficient of $Mg_{3.8}Te_xSb_{2-x}$.

all Te doped samples increased up to 373 K, and then decreased. Seebeck coefficient variation behavior and electrical conductivity in the test temperature range appeared to fit well together, as expected.

The temperature dependence of total thermal conductivity (κ) and lattice thermal conductivity (κ_L) for $Mg_{3.8}Te_xSb_{2-x}$ ($0.00 \le x \le 0.03$) are shown in Fig. 5(a) and 5(b), respectively. For all compositions, the total thermal conductivity is decreased with increasing temperature up to 773 K, and then slightly increased. This behavior can be explained by considering lattice thermal conductivity (κ_L), and electronic thermal conductivity (κ_E). Total thermal conductivity is known to be the sum of κ_L and κ_E, and according to the Wiedemann-Franz law, electronic thermal conductivity can calculate using $\kappa_E = L\sigma T$ (the Lorenz number $L = \pi^2/3(K_B/e)^2 = 2.38 \times 10^{-8}$ $W\Omega K^{-2}$). As shown in Fig. 5(a) and 5(b), the difference between κ and κ_L is very small, which describe the main contributor of κ is κ_L. Due to the high mass difference between Te and Sb, the substitution of Te at Sb sites may initiate point defect scattering, lowering lattice thermal conductivity.[23] Total thermal conductivity is observed to increase at 773 K for all compositions. This is possibly due to an increase in electrical conductivity at that temperature. The decrease in thermal conductivity could be attributed to the doping effect.

Table 1. Relative density and transport properties of vacuum hot pressed $Mg_{3.8}Te_xSb_{2-x}$ samples at room temperature.

Nominal composition $Mg_{3.8}Sb_{2-x}Te_x$	Hall coefficient (cm^3C^{-1})	Carrier mobility ($cm^2V^{-1}s^{-1}$)	Carrier concentration ($\times 10^{16}cm^{-3}$)	Relative Density (%)
x = 0.00	-155.82	0.2650	-0.4391	~ 99.10
x = 0.01	-62.40	0.2325	-2.852	~ 99.20
x = 0.02	-46.74	0.2141	-2.980	~ 99.23
x = 0.03	-35.62	0.2053	-3.256	~ 99.46

The dimensionless figure of merit (ZT) is evaluated in Fig. 6 with respect to temperature and x. Sample $Mg_{3.8}Te_{0.01}Sb_{1.99}$ shows a peak ZT ≈ 0.27 at 873 K due to its relatively lower thermal conductivity and optimum electronic properties. This improvement of ZT is 1.12 times higher than that of the pristine one.

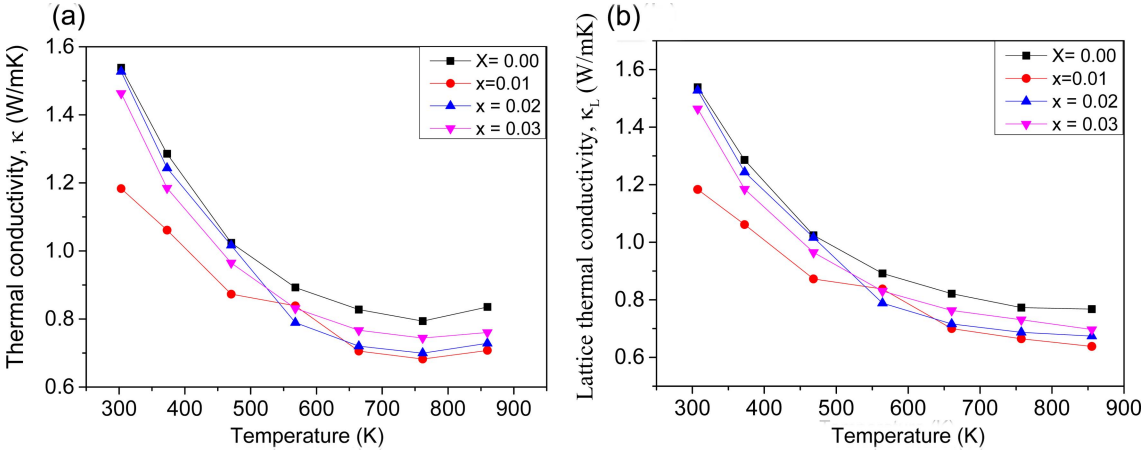

Fig. 5. Temperature dependence of (a) thermal conductivity and (b) lattice thermal conductivity of VHPed $Mg_{3.8}Te_xSb_{2-x}$.

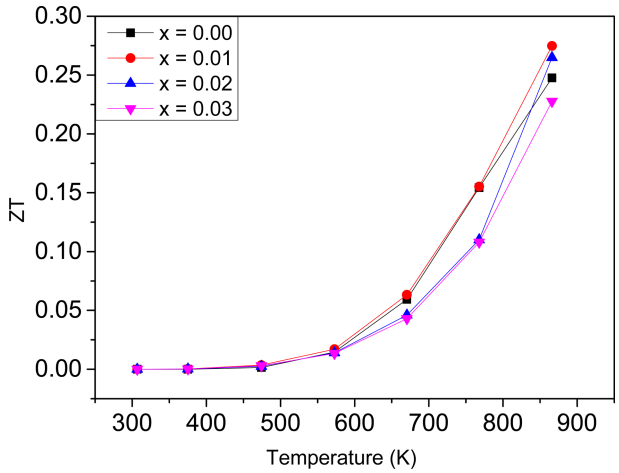

Fig. 6. Temperature dependence dimensionless figure of merit (ZT) of VHPed $Mg_{3.8}Te_xSb_{2-x}$.

4. Conclusion

Nominal compositions of $Mg_{3.8}Te_xSb_{2-x}$ ($0.00 \leq x \leq 0.03$) were successfully synthesized by the controlled melting and subsequent vacuum hot pressing method. Te seemed to be uniformly distributed throughout the matrix and played an important role as a dopant. The substitution of Te at Sb sites has controlled to increase phonon scattering, which is responsible for the reduction in thermal conductivity. The methodical measurement shows the peak ZT value of 0.27 at 873 K. Despite of the fact that this study showed relatively lower thermal conductivity, the acquired electrical conductivity appeared to be quite low due to the lower value of carrier concentration. It is proposed that selective doping could increase carrier concentration even more, potentially increasing ZT value in n-type Mg_3Sb_2.

Acknowledgement

This research was supported by the Korea Basic Science Institute grant funded by the Ministry of Education (grant no. 2019R1A6C1010047).

References

1. A. R. M. Siddique, S. Mahmud and B. V. Heyst, Renew. Sustain. Energ. Rev., **73**, 730 (2017).
2. R. Franz and G. Wiedemann, Ann. Phys., **165**, 497 (1853).
3. H. S. Dow, M. Na, S. J. Kim and J. W. Lee, J. Mater. Chem. C, **7**, 3787 (2019).
4. G. Joshi, H. Lee, Y. Lan, X. Wang, G. Zhu, D. Wang, R. W. Gould, D. C. Cuff, M. Y. Tang, M. S. Dresselhaus, G. Chen and Z. Ren, Nano Lett., **8**, 4670 (2008).
5. Y. Pei, Z. M. Gibbs, A. Gloskovskii, B. Balke, W. G. Zeier and G. J. Snyder, Adv. Energy Mater., **4**, 1400486 (2014).
6. Y. Zhao, J. S. Dyck, B. M. Hernandez and C. Burda, J. Am. Chem. Soc., **132**, 4982 (2010).
7. S. M. Kauzlarich, S. R. Brown and G. J. Snyder, Dalton Trans., **21**, 2099 (2007).
8. Q. G. Cao, H. Zhang, M. B. Tang, H. H. Chen, X. X. Yang, Y. Grin and J. T. Zhao, J. Appl. Phys., **107**, 10 (2010).
9. A. Bhardwaj, N. S. Chauhan, S. Goel, V. Singh, J. J. Pulikkotil, T. D. Senguttuvan and D. K. Misra, Phys. Chem. Chem. Phys., **18**, 6191 (2016).
10. J. Zhang, L. Song, K. A. Borup, M. R. V. Jorgensen and B. B. Iversen, Adv. Energy Mater., **8**, 1 (2018).
11. Y. Wang, X. Zhang, Y. Wang, H. Liu and J. Zhang, Phys. Status Solidi A, **216**, 1 (2019).
12. F. Zhang, C. Chen, H. Yao, F. Bai, L. Yin, X. Li, S. Li, W. Xue, Y. Wang, F. Cao, X. Liu, J. Sui and Q. Zhang, Adv. Funct. Mater., **30**, 1 (2020).
13. L. Song, J. Zhang and B. B. Iversen, J. Mater. Chem. A, **5**, 4932 (2017).
14. A. Bhardwaj, N. S. Chauhan and D. K. Misra, J. Mater. Chem. A, **3**, 10777 (2015).
15. A. Bhardwaj, A. Rajput, A. K. Shukla, J. J. Pulikkotil, A. K. Srivastava, A. Dhar, G. Gupta, S. Auluck, D. K. Misra and R. C. Budhani, RSC Adv., **3**, 8504 (2013).
16. H. Tamaki, H. K. Sato and T. Kanno, Adv. Mater., **28**, 10182 (2016).
17. P. Gorai, B. R. Ortiz, E. S. Toberer and V. Stevanovic, J. Mater. Chem. A, **6**, 13806 (2018).
18. M. M. Rahman, A. K. M. A. Shawon and S.-C. Ur, Electron. Mater. Lett., **17**, 102 (2021).
19. A. K. M. A. Shawon, M. M. Rahman and S.-C. Ur, Electron. Mater. Lett., **16,** 540 (2020).
20. J. Zhang, L. Song and B. B. Iversen, Angew. Chem., **132**, 4308 (2020).
21. M. Dittrich and G. Schumacher, Mater. Sci. Eng., A, **604**, 27 (2014).
22. Y. Cui, X. Zhang, B. Duan, J. Li, H. Yang, H. Wang, P. Wen, T. Gao, Z. Fang, G. Li, Y. Li and P. Zhai, J. Mater. Sci.: Mater. Electron., **30**, 15206 (2019).
23. H. Fujishiro, M. Ikebe, M. Yagi, K. Nakasato, Y. Shibazaki and T. Fukase, J. Low Temp. Phys., **105**, 981 (1996).

Author Information

Md. Mahmudur Rahman
한국교통대학교 대학원 석사수료
Soon-Chul Ur
한국교통대학교 교수